Journal of Nuclear Medicine, published on March 24, 2022 as doi:10.2967/jnumed.121.263189

Phase 1 Evaluation of ^{11}C-CS1P1 to Assess Safety and Dosimetry in Human Participants

Matthew R. Brier[1], Mahdjoub Hamdi[2], Jayashree Rajamanikam[2], Haiyang Zhao[2], Syahir Mansor[2], Lynne Jones[2], Farzaneh Rahmani[2], Saurabh Jindal[2], Deborah Koudelis[2], Joel S. Perlmutter[1,2,3,4], Dean F. Wong[2,1,3,5], Michael Nickels[2], Joseph E. Ippolito[2], Robert J. Gropler[2], Thomas H. Schindler[2], Richard Laforest[2], Zhude Tu[2*], Tammie L. S. Benzinger[2*]

[1]Department of Neurology, [2]Mallinckrodt Institute of Radiology, [3]Neuroscience, [4]Physical and Occupational Therapy, [5]Psychiatry, Washington University in St. Louis

*Corresponding Authors

Correspondence To:

Tammie L.S. Benzinger MD PhD and Zhude Tu, PhD

660 S Euclid Ave

St. Louis, MO 63110

benzingert@wustl.edu & zhudetu@wustl.edu

First Author:

Matthew R. Brier MD PhD

660 S Euclid Ave

St. Louis, MO 63110

brierm@wustl.edu

Word Count: 4,964 words

Funding: NIH

Running Title: CS1P1 Dosimetry

ABSTRACT

Purpose: This study evaluated the safety, dosimetry, and characteristics of ^{11}C-CS1P1, a radiotracer targeting sphingosine-1-phoshate receptor 1. Sphingosine-1-phoshate receptor 1 is of clinical interest because of its role in multiple sclerosis (and other conditions) with an expanding class of sphingosine-1-phosphate receptor modulators approved for relapsing multiple sclerosis. ^{11}C-CS1P1 binds sphingosine-1-phosphate receptor 1 with high specificity and has shown promise in animal models of inflammatory diseases.

Procedures: ^{11}C-CS1P1 was injected into 5 male and 6 female healthy participants. Ten participants were imaged with positron emission tomography using a multi-pass whole-body continuous-bed-motion acquisition and one had dedicated head and neck positron emission tomography and magnetic resonance imaging. Participants were continuously monitored for safety events. Organ time activity data were collected, integrated and normalized to the injected activity. Organ radiation doses as well as effective dose were computed using the adult male and female model in OLINDA v2.2. SUV images were evaluated for qualitative biodistribution.

Results: No adverse events were observed following the dose, including no bradycardia. The liver was the critical organ from dosimetry analysis (mean ± st. dev; Female: 23.12 ± 5.19 μSv/MBq; Male: 21.06 ± 1.63 μSv/MBq). The whole-body effective dose (as defined by ICRP103) was 4.18 ± 0.30 μSv/MBq in females and 3.54 ± 0.14 μSv/MBq in males. Using a maximum delivered dose of 740 MBq (20 mCi), the effective dose for females would be 3.1 mSv (0.31 rem) with a liver dose of 17.1 mSv (1.7 rem); the effective dose for males would be 2.6 mSv (0.26 rem) with a liver dose of 15.6 mSv (1.56 rem). Brain uptake was predominantly seen in gray matter and correlated with regional sphingosine-1-phosphate receptor 1 RNA expression (r = 0.84).

Conclusions: These results support the safety of ^{11}C-CS1P1 for evaluation of inflammation in human clinical populations. Dosimetry permits repeated measures in the same participants. Brain uptake correlates well with known target topography.

Key words: spingosine-1-phosphate, spingosine-1-phosphate receptors, positron emission tomography, cerebral inflammation, radiation dosimetry.

INTRODUCTION

Sphingosine-1-phosphate (S1P) is a membrane derived lysophospholipid that plays a regulatory role in inflammatory diseases including multiple sclerosis (MS) (*1*) and inflammatory bowel disease (*2*). S1P signals via five G protein-coupled receptors (S1PR1-5) (*3*). S1PR1 is expressed on a variety of tissues including endothelial cells, vascular smooth muscle cells, astrocytes, and lymphocytes (*4*,*5*). Treatment with any of four Food and Drug Administration approved S1PR1 modulators sequesters lymphocytes within lymph nodes (*6*) thereby reducing relapses in MS patients (*7*). In addition to lymphoid effects, S1PR1 modulation also inhibits microglial activation (*8*), improves remyelination following injury (*9*), and promotes oligodendrocyte survival (*5*), presumably mediated by astrocyte signaling (*10*). Thus, in vivo imaging of S1PR1 could contribute to the understanding of MS and other inflammatory disorders, including response to treatment.

S1PR1 signaling plays an important role beyond prototypic inflammatory disorders. For example, high S1PR1 expression relates to higher mortality in estrogen receptor positive breast cancer (*11*). Similarly, S1PR1 partially regulates neovascularization of tumors (*12*) and modulates expression of hypoxia-inducible factor 2 alpha, which can drive aggressive malignancy (*13*).

A recently developed radiotracer, ^{11}C-CS1P1, shows increased binding in an experimental autoimmune encephalomyelitis (EAE) rodent model (*4*), following carotid artery injury (*14*), and within atherosclerotic plaques (*15*). Safety and dosimetry studies in a rodent model demonstrated good safety and low radiation dose exposure compatible with first-in-human testing (*16*). This paper reports on the safety, radiation dosimetry, and initial imaging results of ^{11}C-CS1P1 in eleven healthy human volunteers.

MATERIALS AND METHODS

Study Design and Participants

This study was pre-registered on ClinicalTrials.gov (NCT04517552), approved by the Washington University Institutional Review Board and Radioactive Drug Research Committee, and performed under Food and Drug Administration IND 146548. All participants provided written informed consent. The "dosimetry cohort" consisted of ten healthy participants (5 male / 5 female) who underwent whole body PET/CT imaging. Additionally, one female participant underwent dedicated brain imaging. Inclusion criteria were 1) male or female, any race, 2) age greater than 18 years old, 3) capable of providing written informed consent to undergo research procedures, 4) a generally healthy individual without major neurological disease (e.g., epilepsy). Exclusion criteria included 1) hypersensitivity to ^{11}C-CS1P1 or any of its excipients, 2) contraindications to PET or CT, 3) severe claustrophobia, 4) women who are pregnant or breastfeeding, 5) conditions that could increase risk of study participation (e.g., renal or liver failure), 6) currently undergoing radiation therapy, or 7) history of unstable arrhythmias or indications of cardiovascular disease. The cardiac-related exclusion derives from the association between S1P-modulating drugs and clinically significant bradycardia (*7*), despite the small injected mass of radiopharmaceutical.

Radiopharmaceutical Synthesis

The radiosynthesis of ^{11}C-CS1P1 was accomplished by alkylating the precursor with ^{11}C-methyl triflate in acetonitrile at 60 ˚C for 5 minutes, followed by removal of the t-butyl group using trifluoroacetic acid, and purification using reverse phase high-performance liquid chromatography (*17*).

Dosimetry Cohort PET/CT Image Acquisition

Ten dosimetry participants were imaged using a Biograph Vision PET/CT (Siemens Healthineers). A low-dose CT was performed from the vertex to mid-thigh prior to PET imaging for anatomical alignment and attenuation correction (120 kVp, 50 mAs). Following injection of ^{11}C-CS1P1 and a saline flush, dynamic images were obtained over the heart for 5 minutes followed by whole-body dynamic acquisitions in continuous bed motion. Acquisition only involving the heart for the first five minutes was done for two reasons. First, to allow for capturing the high amount of radioactivity in the blood volume in the heart immediately following injection and, second, to facilitate the required electrocardiogram. Whole-body sweep epochs were 120s (x11), 300s (x6), and 600s (x6) over approximately 2 hours using continuous bed motion acquisition. PET images were reconstructed using a 3D ordered subset expectation maximization algorithm (3D-OSEM) with time-of-flight and point spread functions resolution modeling (4 iterations/5 subsets) with no post-reconstruction filtering. Images were inspected for evidence of motion and alignment was manually corrected, if needed.

Pharmaceutical Safety Evaluation

Safety of the injected dose was assessed in several ways. First, serial electrocardiograms (at enrollment, prior to injection, 5 min after injection, and then hourly until discharge) were performed and the patient was monitored on telemetry to assess for bradycardia (HR < 40 bpm) or other significant arrhythmias (atrial fibrillation or flutter, re-entrant tachycardia, 2nd or 3rd degree heart block, or ventricular arrhythmia). Similarly, patients were monitored for hypotension (SBP < 100, DBP < 70). Laboratory evaluation following injection consisted of a complete blood count, comprehensive metabolic panel and urinalysis and were compared to baseline measures. Finally, all participants were contacted 2 – 3 days following the study to assess for any delayed adverse events.

Qualitative Biodistribution

Whole-body CT scans received standard-of-care review by a board-certified radiologists (TLSB and JI). Following image acquisition, merged CT and ^{11}C-CS1P1 PET images were re-reviewed (MRB, TLSB and JI) to identify potential findings of interest regarding ^{11}C-CS1P1.

Radiation Dosimetry

Volumes of interest (VOI) were manually traced over source organs with measurable activity: brain, lungs, cardiac muscle, lung, liver, spleen, kidney, small intestine, urinary bladder and muscle. Organs with well-defined boundaries were contoured in their entirety (e.g., liver, kidneys). Organs with complex boundaries (e.g., small bowel) or impacted by respiratory motion (e.g., heart, lungs) were sampled and activity scaled to the estimated mass of the organ. Time-activity curves were obtained for each source organ by expressing the total activity (non-decay corrected) in the VOI as a percentage of total injected activity. Numerically integrated time-activity values were entered into OLINDA 2.2 (Hermes) to calculate organ doses and effective dose (as defined by ICRP-103) (*18*) using the ICRP-89 (*19*) adult human male and female models.

Owing to the acquisition of dynamic images only involving the heart during the first five minutes, the brain, muscle, and urinary bladder were outside the field of view. Small bowel was sampled such that the VOI was within the field of view. Time activity curves were linearly interpolated from time of injection to the first measurement with the organ in the field of view.

Minimal urinary excretion was observed with low activity collecting in the urinary bladder consistent with the previous rodent data (*16*). Thus, no excretion was modeled. Only physical decay was assumed after the last measurement. The body remainder was determined by subtracting all source organs from the calculated maximum integrated time activity value of ^{11}C calculated from the reciprocal of the decay constant.

Dedicated Brain PET/CT and MRI Image Acquisition and Processing

One additional participant underwent dedicated head and neck imaging using a Biograph Vision PET/CT (Siemens). A low-dose CT was performed from the vertex to the cervicothoracic junction for anatomical alignment and attenuation correction. Following injection of ^{11}C-CS1P1 and a saline flush, dynamic images were obtained from the vertex to about C5 for two-hours. The participant took a 15-minute break after 60 minutes. PET images were reconstructed using a 3D ordered subset expectation maximization algorithm (3D-OSEM) with time-of-flight and point spread functions resolution modeling (8 iterations/5 subsets). For the purposes of this analysis, frames from 30 min to 60 min were summed to create summed activity images and converted to a standardized uptake value image using the participants measured body weight for normalization.

This participant also underwent 3 Tesla head and neck MRI scanning (Siemens Biograph mMR) using a 32-channel head and neck coil. A T1 weighted MPRAGE and T2 weighted 3D FLAIR image were acquired for image registration and segmentation. The MPRAGE and FLAIR image were processed through FreeSurfer (*20*) v7.2 which identifies brain structures in a semi-automated manner. FreeSurfer segmentation and the summed activity images were aligned through affine registration (in-house software, https://4dfp.readthedocs.io) and the SUVs extracted from labelled regions. RNA expression, defined by microarray and expressed as Z-scores, were downloaded from the Allen Brain Atlas (2010) for *S1PR1*, *2*, *3*, *4*, and *5*. Regions defined in both FreeSurfer and Allen Brain Atlas and measurable without explicit partial volume correction were extracted.

Statistical Analysis

Mean and standard deviations for all measurements across individuals are provided. Males and females are reported separately. We also compared the relationship between RNA expression (expressed as Z-scores from the Allen Brain Atlas) and ^{11}C-CS1P1 activity using a Pearson r test.

RESULTS

Participant Characteristics and Injected Dose

Table 1 provides demographic and radiopharmaceutical dosing information for the ten dosimetry participants. The mean and standard deviation of the administered mass of ^{11}C-CS1P1 was 3.15 μg ± 0.98 μg (range 0.98 μg – 4.70 μg). The mean administered activity was 226.4 MBq ± 71.97 MBq (range 99.9 MBq – 362.6 MBq).

Safety Events

There were no adverse or clinically detectable pharmacologic effects in any of the participants. No participants reported adverse reactions immediately following the scan. One participant reported mild flu-like symptoms at the follow up call. No participants reported headache, injection site reactions, or symptoms consistent with bradycardia.

No events of asymptomatic or symptomatic bradycardia, hypotension (SBP < 100, DBP < 70), arrhythmias, or changes in complete blood count, comprehensive metabolic panel, or urinalysis were observed. Pre-injection, 5-minute post-injection, and discharge heart rate captured on 12 lead electrocardiogram were stable in all participants (Figure 1).

Qualitative Bio-distribution (Dosimetry Cohort)

Male and female decay-corrected, summed activity images demonstrate significant uptake by the liver and, to a much lesser extent, kidneys (Figure 2A). At early time points, high activity was seen in the liver and at later points concentrated in the gallbladder (Figure 2B). Activity accumulated in the small bowel at late time points but since significant decay has occurred by 120 minutes (approximately 6 half-lives) post-injection, radiation dose to the small intestine was minimal. These observations are

compatible with hepatobiliary clearance. Minimal activity was observed in the urinary bladder or in the excreted urine (average urinary activity 2.67 MBq).

^{11}C-CS1P1 uptake was next examined in more detail throughout the body (Figure 3). Brain uptake was higher in gray matter, including subcortical structures, compared to white matter (Figure 3A). Notably, spinal uptake was minimal. Increased uptake was observed in the submandibular salivary glands (Figure 3B), left ventricle (Figure 3C), liver and common bile duct (Figure 3D). Low levels of activity were seen in the kidneys and the urinary bladder. No enlarged lymph nodes were identified in the 10 dosimetry participants.

Integrated Time Activity

Integrated time activity was calculated in organs demonstrating measurable activity (Figure 4; Table 2). The highest integrated time activity was seen in the liver (6.37 ± 1.11 minutes). The mean integrated time activity of muscle was 5.51 ± 0.98 minutes (21% of injected dose) and assigned to the remainder of the body in the OLINDA2.2 model. Other notable organs include the kidney (0.92 ± 0.22 minutes) but minimal measurable integrated time activity in the urinary bladder (0.01 ± 0.02 minutes). A large fraction of the integrated time activity was not measured in a specific organ (specifically measured: 34%, unmeasured: 66%) and thus distributed into the remainder of the body.

Dosimetry

Dosimetry tables for females (Table 3) and males (Table 4) show the dose distribution calculated using OLINDA2.2. The dose limiting organ was the liver with a dose of 23.12 μSv/MBq in females and 21.06 μSv/MBq in males. The Effective Dose was 4.18 μSv/MBq in females and 3.54 μSv/MBq in males. Using a maximum delivery dose of 740 MBq (20 mCi), the Effective Dose for females would be 3.1 mSv (0.31 rem) with a liver dose of 17.1 mSv (1.7 rem); the Effective Dose for males would be 2.6 mSv (.26 rem) with a liver dose of 15.6 mSv (1.56 rem).

Brain-specific Activity Analysis

The summed decay-corrected activity measured from 30- to 60-minutes post-injection a single participant is shown in Figure 5. Gray matter, specifically subcortical gray matter, had higher activity than white matter. Within gray matter, visual cortex has relatively high activity while the temporal pole and medial temporal lobe had low activity. On the basis of a single participant, we present preliminary evidence that ^{11}C-CS1P1 selectively accumulates in brain regions that express S1PR1. In a small set of regions of interest, we found a strong correlation (r = 0.84, P = 0.016) between ^{11}C-CS1P1 activity (expressed as a Z-score compared to whole brain activity) and *S1PR1* RNA expression (expressed as a Z-score) obtained from the Allen Brain Atlas (Figure 6). We assessed the specificity of ^{11}C-CS1P1 for S1PR1 by examining the correlation between ^{11}C-CS1P1 binding and RNA expression of S1P[2-5]. We found much weaker correlations with off-target S1P-receptors compared to S1PR1 (Figure 7; r = 0.85 vs. r < 0.57). These results suggest that ^{11}C-CS1P1 is successfully engaging the target in a specific manner.

DISCUSSION

We report the safety and dosimetry of intravenous administration of ^{11}C-CS1P1 to healthy human volunteers. No safety events were observed following injection. Dosimetry analysis revealed effective doses within acceptable limits, including the critical organ (liver). These results support the safety of ^{11}C-CS1P1 for human investigation.

S1PR1 modulating drugs, such as fingolimod, are approved for the treatment of relapsing-remitting MS. These drugs are highly efficacious but fingolimod was associated potentially significant bradycardia (*7*). The drug label requires cardiac monitoring for the first dose and, consequently, there was concern that ^{11}C-CS1P1 could similarly cause bradycardia despite the very low mass of CS1P1 injected. This safety study collected frequent electrocardiograms and telemetry monitoring and found

no significant bradycardia or conduction abnormalities. Such abnormalities were not expected owing to the low mass of ^{11}C-CS1P1 injected (3.15 ± 0.98 μg compared to fingolimod dose of 0.5 mg). In fact, heart rate tended to increase over the study strongly suggesting a negligible effect of ^{11}C-CS1P1 on cardiac conduction. Finally, no significant laboratory abnormalities were identified. Thus, we conclude that, given the present exclusion criteria, ^{11}C-CS1P1 is a safe and well-tolerated radiotracer.

The critical organ was the liver, consistent with rodent dosimetry studies (*16*). Liver integrated time activity was 6.37 min and 8.34 min in in the human and mouse, respectively. The calculated effective dose based on human measurement was 4.18 μSv/MBq in females and 3.54 μSv/MBq in males. For an injected dose of 740 MBq (20 mCi), the whole-body effective dose would be 3.1 mSv (0.31 rem) for females and 2.6 mSv (0.26 rem) for males. The liver effective dose would be 17.1 mSv (1.71 rem) for females and 15.6 mSv (1.56 rem) for males. As a comparison, the effective dose of ^{11}C-PIB, a well-known marker of amyloid-β deposition in the brain associated with Alzheimer's disease, is 4.74 μSv/MBq (*21*). This effective dose supports the safety and utility of ^{11}C-CS1P1 for human imaging from a radiation dose perspective.

The first 5 minutes of PET data were collected over the thorax to capture initial blood radioactivity and facilitate safety procedures. Thus, counts from some organs (e.g., brain) were not collected and were imputed for the early time points. This imputation was performed by linear interpolation from the injection time to the earliest measured time point. Other interpolation strategies were possible; however such choices are arbitrary and would not meaningfully influence the calculated dosimetry. For example, the brain is the organ outside the initial field of view with the highest uptake but only represents ~1.5% of the total activity in the post-5 minute interval. Thus, the choice to image initially over the thorax did not significantly impact the dosimetry calculation.

Review of CT images revealed no incidental abnormalities associated with increased ^{11}C-CS1P1 binding. However, the whole-body PET images informs the biology of the tracer. ^{11}C-CS1P1 is clearly metabolized by the liver. This conclusion is supported by the high liver activity, late activity identified in the gallbladder, and the clear identification of the common bile duct on the basis of radioactivity. Renal uptake is likely not related to clearance since the collecting systems have little activity and only a small amount of activity was collected in the urinary bladder. Significant activity is also seen within the cardiac muscle and S1P-based signaling is known to contribute to dose-related bradycardia in fingolimod (*7*). Salivary gland activity may be related to the role of S1P-signaling in pathology of salivary glands such as Sjogren's syndrome (*22*).

Finally, we present preliminary evidence in a single participant that ^{11}C-CS1P1 selectively accumulates in brain regions that have greater S1PR1 expression. Ongoing work in a larger cohort will determine whether this finding can be confirmed. We note that this finding is compatible with animal work that demonstrate similar tracer behavior in animals (*4*).

CONCLUSION

We present human safety and dosimetry data supporting the application of ^{11}C-CS1P1 to the study of human disease. This radioligand is well tolerated from both a medical and radiological perspective. Future studies will explore the utility of this tracer for the study of multiple sclerosis and other inflammatory diseases.

ACKNOWLEDGEMENTS

This work was supported the USA National Institutes of Health (NIH) from R01NS103988, R01AG054567, P01AG003991, and U19 AG032438, and through National Institute of Neurological

Disorders and Stroke, National Institute on Aging (NS103988, NS107281, and NS075527). MRB was supported by 2R25NS090978-06. DFW was supported by the National Institute of Mental Health (7R01MH10719705). JSP was supported by the Barnes Jewish Hospital Foundation (Stein Family Fund), Riney Foundation, N William Grant Fund, American Parkinson Disease Association (APDA) and the Greater St. Louis Chapter of the APDA. No potential conflicts of interests relevant to this article exist.

KEY POINTS

Question: Is ^{11}C-CS1P1 safe for use in human imaging?

Pertinent Findings: ^{11}C-CS1P1 was not associated with any adverse effect. Dosimetry is compatible with longitudinal human imaging.

Implications for Patient Care: ^{11}C-CS1P1 is safe for human use and can be used to study inflammation in disease such as multiple sclerosis.

REFERENCES

1. Proia RL, Hla T. Emerging biology of sphingosine-1-phosphate: Its role in pathogenesis and therapy. *Journal of Clinical Investigation*. 2015;125:1379-1387.

2. Peyrin-Biroulet L, Christopher R, Behan D, Lassen C. Modulation of sphingosine-1-phosphate in inflammatory bowel disease. *Autoimmunity Reviews*. 2017;16:495-503.

3. Lee MJ, van Brocklyn JR, Thangada S, et al. Sphingosine-1-phosphate as a ligand for the G protein-coupled receptor EDG-1. *Science*. 1998;279:1552-1555.

4. Liu H, Jin H, Yue X, et al. PET Imaging Study of S1PR1 Expression in a Rat Model of Multiple Sclerosis. *Molecular Imaging and Biology*. 2016;18:724-732.

5. Jackson SJ, Giovannoni G, Baker D. Fingolimod modulates microglial activation to augment markers of remyelination. *Journal of Neuroinflammation*. 2011;8:1-12.

6. MacEyka M, Spiegel S. Sphingolipid metabolites in inflammatory disease. *Nature*. 2014;510:58-67.

7. Kappos L, Antel J, Comi G, et al. Oral Fingolimod (FTY720) for Relapsing Multiple Sclerosis. *New England Journal of Medicine*. 2006;355:1124-1140.

8. Brinkmann V. FTY720 (fingolimod) in Multiple Sclerosis: Therapeutic effects in the immune and the central nervous system. *British Journal of Pharmacology*. 2009;158:1173-1182.

9. Miron VE, Ludwin SK, Darlington PJ, et al. Fingolimod (FTY720) enhances remyelination following demyelination of organotypic cerebellar slices. *American Journal of Pathology*. 2010;176:2682-2694.

10. Choi JW, Gardell SE, Herr DR, et al. FTY720 (fingolimod) efficacy in an animal model of multiple sclerosis requires astrocyte sphingosine 1-phosphate receptor 1 (S1P1) modulation. *Proceedings of the National Academy of Sciences of the United States of America*. 2011;108:751-756.

11. Watson C, Long JS, Orange C, et al. High expression of sphingosine 1-phosphate receptors, S1P1and S1P3, sphingosine kinase 1, and extracellular signal-regulated kinase-1/2 is associated with development of tamoxifen resistance in estrogen receptor-positive breast cancer patients. *American Journal of Pathology*. 2010;177:2205-2215.

12. LaMontagne K, Littiewood-Evans A, Schnell C, et al. Antagonism of sphingosine-1-phosphate receptors by FTY720 inhibits angiogenesis and tumor vascularization. *Cancer Research*. 2006;66:221-231.

13. Sukocheva O, Wadham C, Gamble J, Xia P. Sphingosine-1-phosphate receptor 1 transmits estrogens' effects in endothelial cells. *Steroids*. 2015;104:237-245.

14. Liu H, Jin H, Yue X, et al. PET study of sphingosine-1-phosphate receptor 1 expression in response to vascular inflammation in a rat model of carotid injury. *Molecular Imaging*. 2017;16.

15. Liu H, Jin H, Han J, et al. Upregulated Sphingosine 1-Phosphate Receptor 1 Expression in Human and Murine Atherosclerotic Plaques. *Molecular Imaging and Biology*. 2018;20:448-456.

16. Liu H, Laforest R, Gu J, et al. Acute Rodent Tolerability, Toxicity, and Radiation Dosimetry Estimates of the S1P1-Specific Radioligand [11C]CS1P1. *Molecular Imaging and Biology*. 2020;22:285-292.

17. Luo Z, Gu J, Dennett RC, et al. Automated production of a sphingosine-1 phosphate receptor 1 (S1P1) PET radiopharmaceutical [11C]CS1P1 for human use. *Applied Radiation and Isotopes*. 2019;152:30-36.

18. The 2007 Recommendations of the International Commission on Radiological Protection. ICRP publication 103. *Annals of the ICRP*. 2007;37:1-332.

19. Basic anatomical and physiological data for use in radiological protection: reference values. A report of age- and gender-related differences in the anatomical and physiological characteristics of reference individuals. ICRP Publication 89. *Annals of the ICRP*. 2002;32:5-265.

20. Fischl B. FreeSurfer. *NeuroImage*. 2012;62:774-781.

21. Scheinin NM, Tolvanen TK, Wilson IA, Arponen EM, Någren KÅ, Rinne JO. Biodistribution and radiation dosimetry of the amyloid imaging agent 11C-PIB in humans. *Journal of Nuclear Medicine*. 2007;48:128-133.

22. Seo J, Koo NY, Choi WY, et al. Sphingosine-1-phosphate signaling in human submandibular cells. *Journal of Dental Research*. 2010;89:1148-1153.

Figure 1. Heart Rate Response to 11C-CS1P1 Injection. Stable pre-injection, 5 minute after injection, and discharge heart rate captured on 12-lead electrocardiogram ($p > 0.1$).

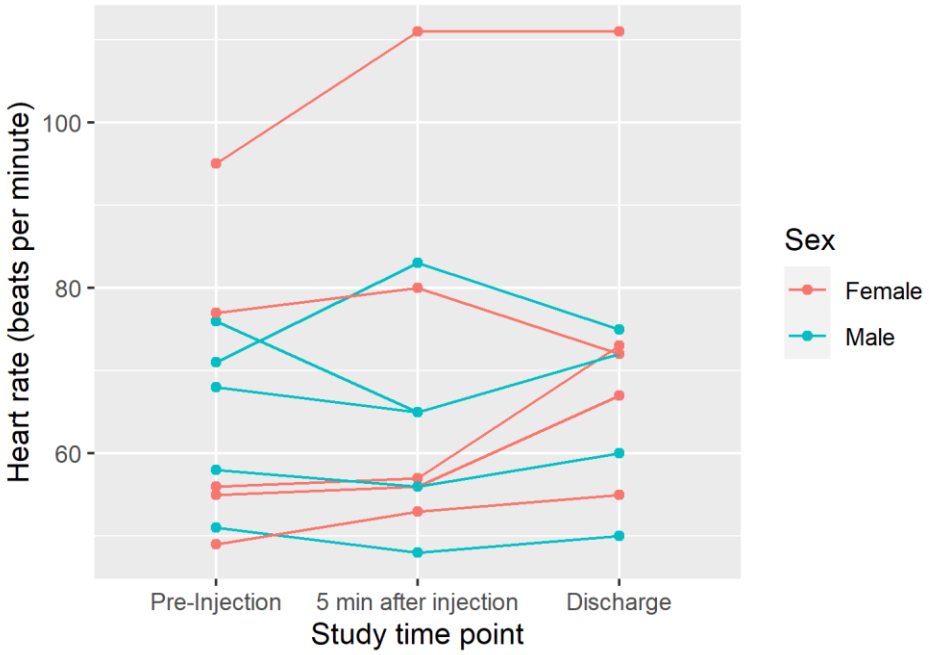

Figure 2. Qualitative Biodistribution of ^{11}C-CS1P1. A) Summed activity images for a representative male and representative female participant. B) Decay corrected activity is high in the liver early in the scanning session but is clearly concentrated in the gallbladder later in the scans, compatible with hepatobiliary excretion.

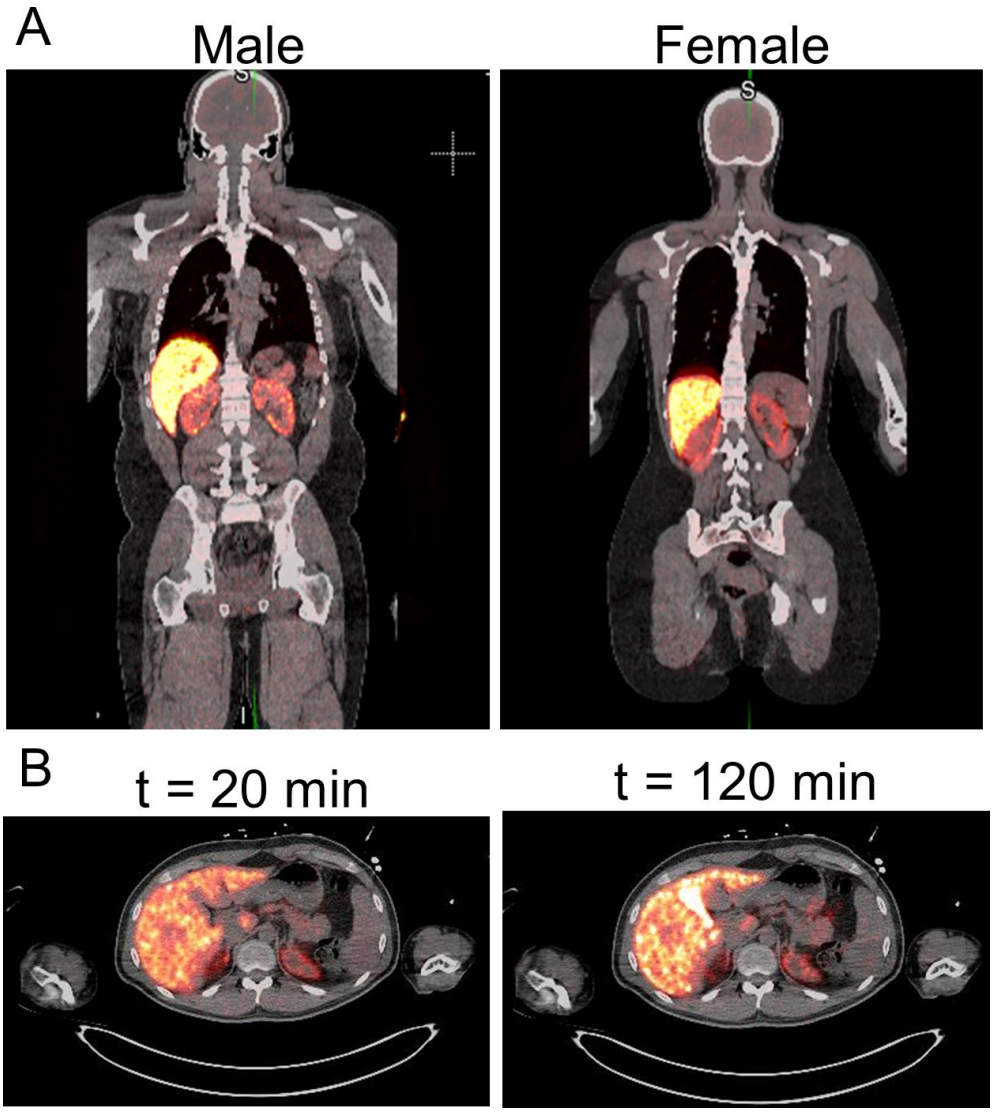

Figure 3. Qualitative biodistribution in a Typical Participant. Summed activity expressed as standardized uptake value (SUV). A) Uptake in the brain is highest in gray matter and relatively low in white matter. Increased update is seen in the salivary glands (B), left ventricle (C) and liver (D). The common bile duct is appreciated (blue arrowhead). E) Paranchymal uptake within the kidneys is seen but without activity in the collecting system with scant amounts of small bowel uptake.

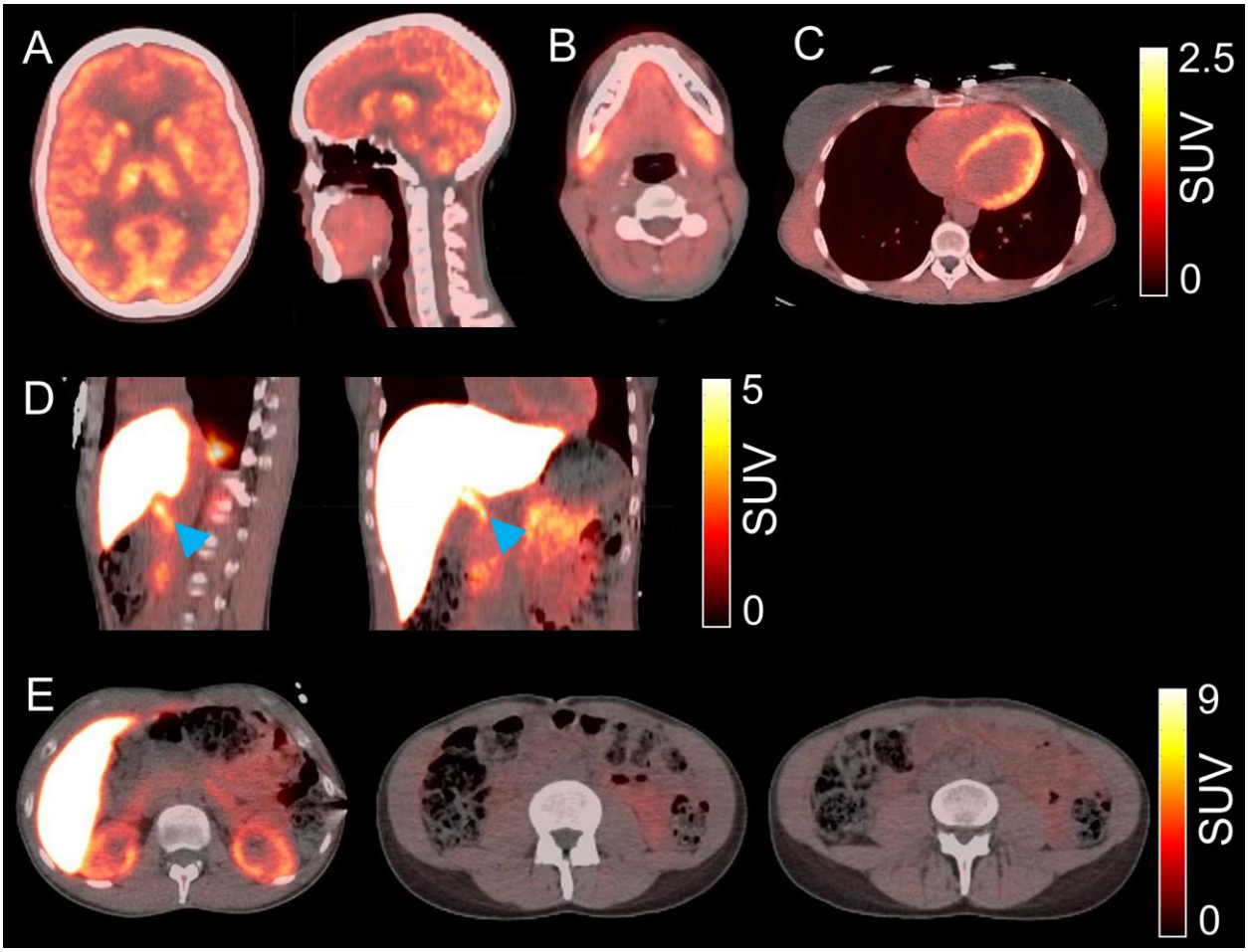

Figure 4. Time Activity Curves. Non-decay (blue) and decay-corrected (red) time activity curves for the organs showing measurable signal. Note that the axes vary in scale by row. The shaded area indicates the first five minutes of the scan when dynamic images over the heart were acquired.

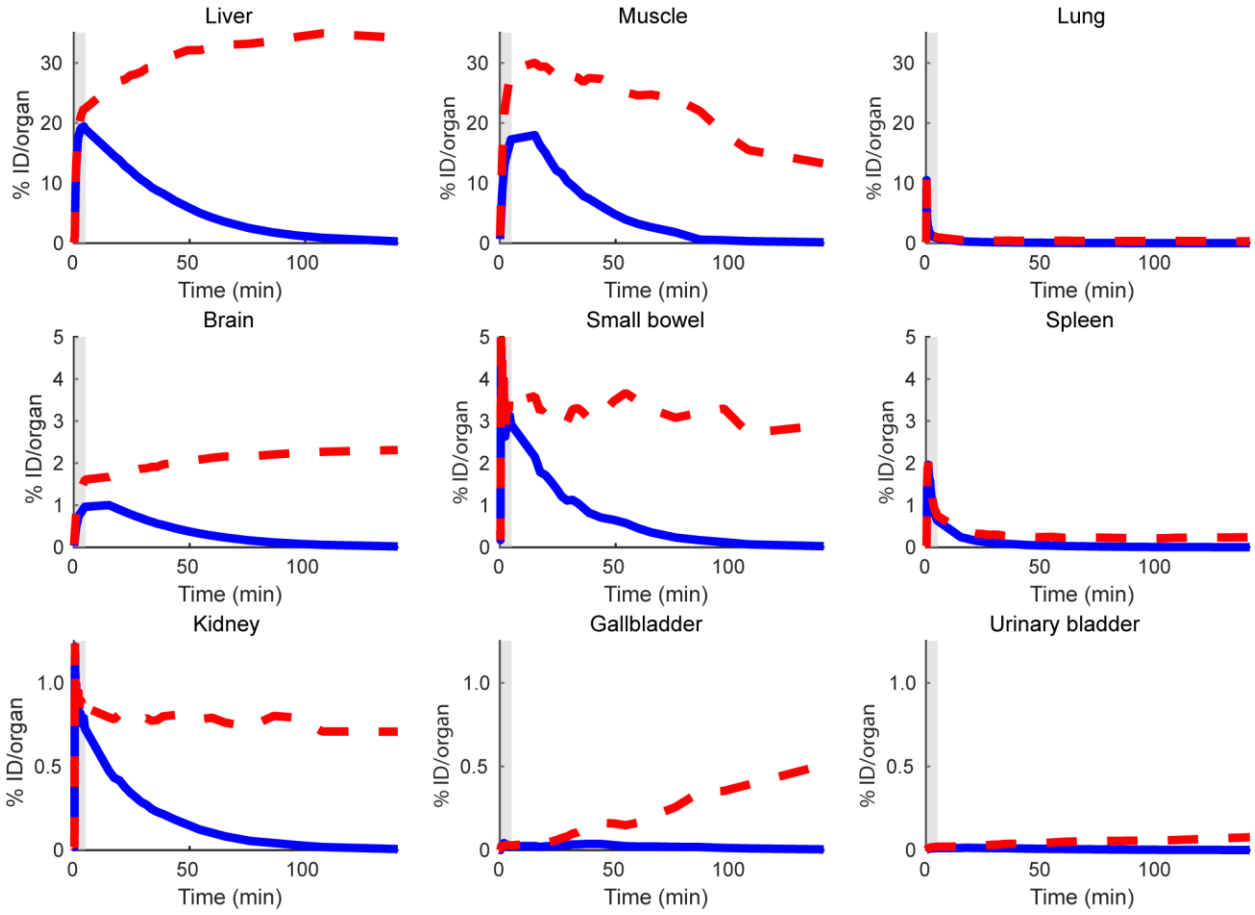

Figure 5. Brain Activity. Summed activity images from 20- to 60-minutes post injection in a single participant with dedicated brain image is shown. Units are SUV based on measured body-weight.

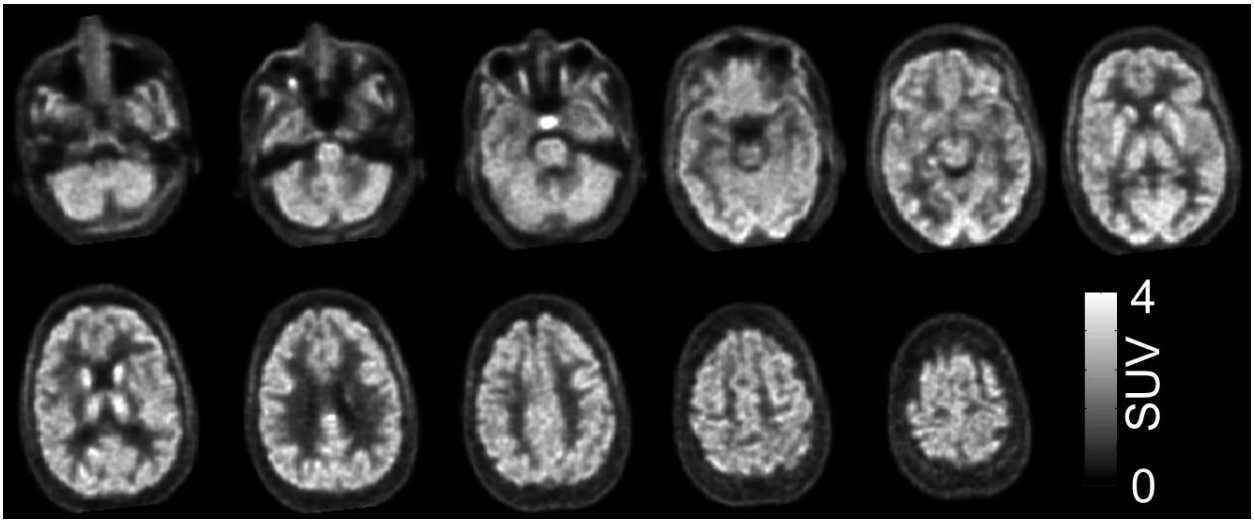

Figure 6. ^{11}C-CS1P1 Uptake is Correlated with S1PR1 Expression. Regional SUV values were extracted from the summed activity image using FreeSurfer and then Z-transformed. Matching S1PR1 RNA expression were extracted from the Allen Brain Atlas and correlated. Tracer activity and RNA expression were significantly correlated thus providing preliminary evidence that ^{11}C-CS1P1 engages its target.

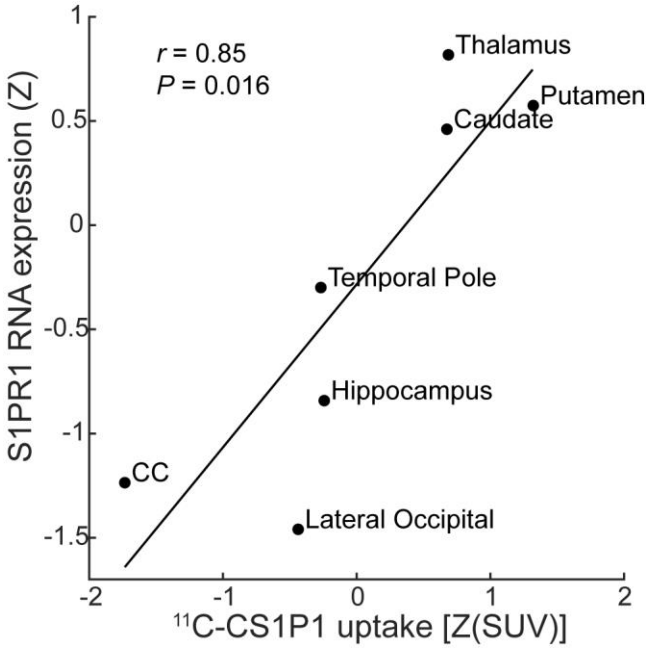

Figure 7. ^{11}C-CS1P1 Uptake is Not Correlated with S1PR[2-5] Expression. Scatter plots in the same style as Figure 6 are shown. All correlations are smaller than the correlation between ^{11}C-CS1P1 and S1PR1.

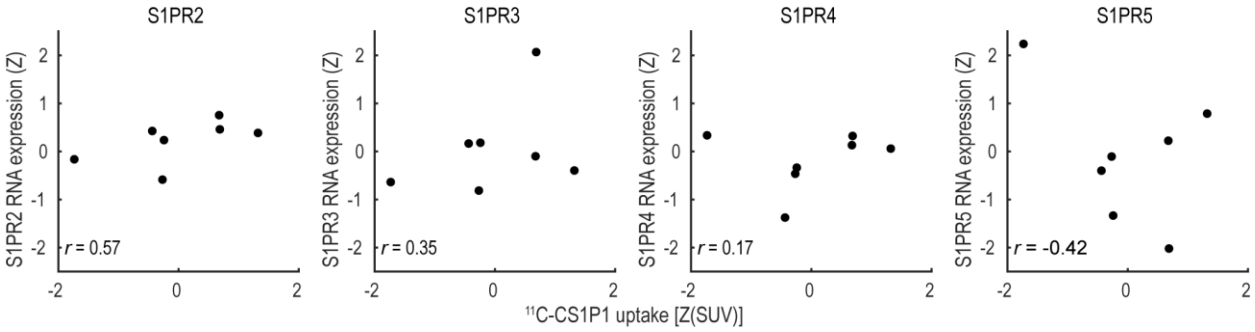

Graphical Abstract

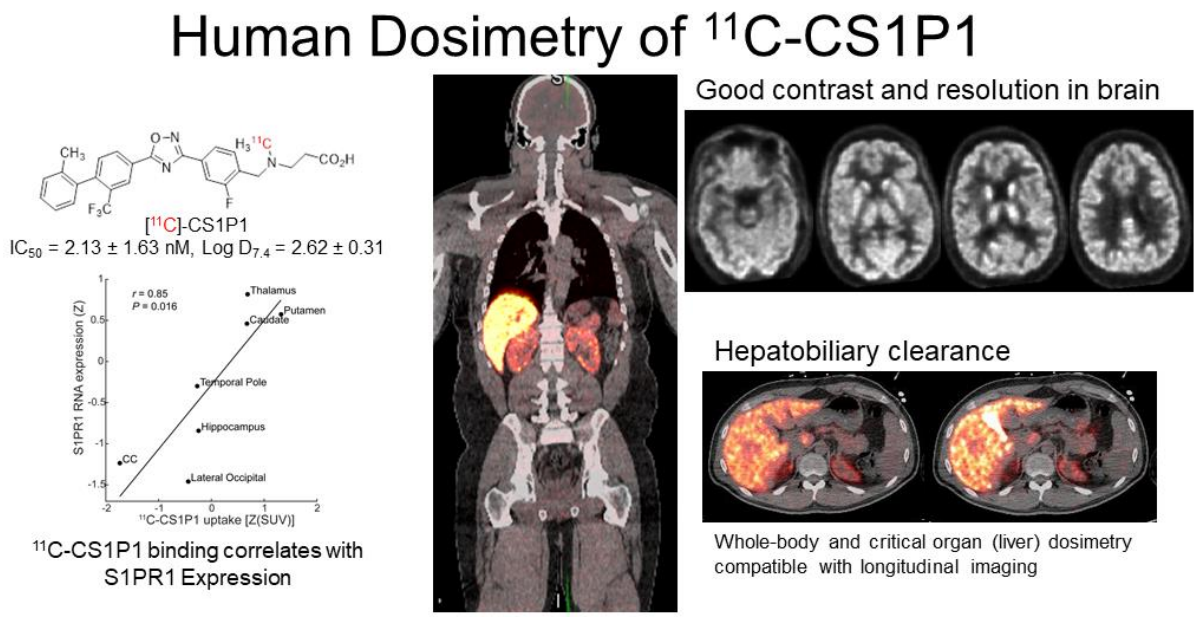

TABLES

Table 1: Participant Demographics and Injected Dose

Participant #	**1**	**2**	**3**	**4**	**5**	**6**	**7**	**8**	**9**	**10**
Sex	M	F	F	M	M	M	M	F	F	F
Age (years)	28	23	40	61	59	34	37	27	27	39
Height (cm)	185.4	177.8	165.1	167.6	185.4	175.3	172.7	165.1	162.6	175.3
Weight (Kg)	88.9	105.7	69.4	67.1	104.8	106.1	74.8	117.9	50.3	117.5
Injected Dose (MBq)	266.4	99.9	170.2	247.9	240.5	296.0	225.7	210.9	362.6	144.3
Injected Dose (mCi)	7.2	2.7	4.6	6.7	6.5	8.0	6.1	5.7	9.8	3.9
Injected Mass (μg)	4.70	4.56	3.29	2.88	2.69	3.40	2.94	3.27	2.78	0.98

Table 2: Integrated Time Activity (minutes)

Participant	1	2	3	4	5	6	7	8	9	10	Avg.	St. Dev
Liver	6.45	5.15	6.85	6.75	6.16	7.41	7.36	4.24	7.76	5.55	6.37	1.11
Brain	0.45	0.39	0.61	0.40	0.38	0.43	0.49	0.29	0.27	0.43	0.41	0.10
Kidney	1.01	0.79	1.22	0.90	0.78	1.15	0.99	0.52	1.09	0.71	0.92	0.22
Small Bowel	0.73	0.66	0.83	1.00	0.88	0.77	0.98	0.35	0.74	0.94	0.79	0.19
Lung	0.29	0.24	0.24	0.23	0.20	0.31	0.27	0.21	0.25	0.19	0.24	0.04
LV Wall	0.16	0.85	0.19	0.28	0.27	0.31	0.31	0.12	0.28	0.18	0.30	0.21
Spleen	0.10	0.08	0.12	0.09	0.10	0.10	0.12	0.07	0.07	0.17	0.10	0.03
Gallbladder	0.01	0.02	0.02	0.01	0.01	0.02	0.03	0.01	0.03	0.02	0.02	0.01
Urinary Bladder	0.01	0.00	0.02	0.01	0.02	0.06	0.01	0.01	0.01	0.01	0.01	0.02
Remainder	16.82	19.06	16.23	17.68	18.45	16.85	15.51	22.27	16.99	19.65	17.95	1.98

Table 3. Radiation dosimetry – Female

	Single Participant Individual Organ Dose (μSv/MBq)						
Participant #	**2**	**3**	**8**	**9**	**10**	**Mean**	**St. Dev**
Adrenals	5.68	6.56	5.28	6.77	6.07	6.07	0.61
Brain	2.06	2.89	1.75	1.57	2.25	2.10	0.51
Breasts	2.44	2.16	2.62	2.29	2.44	2.39	0.17
Esophagus	3.79	3.47	3.46	3.77	3.52	3.60	0.16
Eyes	2.20	1.98	2.50	1.95	2.28	2.18	0.23
Gallbladder Wall	5.88	6.54	5.01	7.28	5.92	6.13	0.84
Left colon	3.47	3.07	3.55	3.21	3.40	3.34	0.20
Small Intestine	3.26	3.13	3.46	3.25	3.43	3.31	0.14
Stomach Wall	3.50	3.31	3.61	3.48	3.56	3.49	0.11
Right colon	12.40	14.70	8.35	13.50	16.40	13.07	3.03
Rectum	2.82	2.47	3.25	2.57	2.92	2.81	0.31
Heart Wall	16.00	5.03	3.93	6.70	4.94	7.32	4.95
Kidneys	14.70	21.90	10.40	20.00	13.70	16.14	4.72
Liver	20.30	26.60	16.90	30.00	21.80	23.12	5.19
Lungs	3.12	3.00	2.73	3.22	2.78	2.97	0.21
Ovaries	2.97	2.64	3.36	2.74	3.08	2.96	0.29
Pancreas	4.75	5.04	4.68	5.39	4.95	4.96	0.28
Salivary Glands	2.35	2.09	2.66	2.09	2.42	2.32	0.24
Red Marrow	2.62	2.42	2.81	2.54	2.67	2.61	0.15
Osteogenic Cells	2.26	2.06	2.48	2.13	2.31	2.25	0.16
Spleen	4.68	6.08	4.08	4.43	7.68	5.39	1.49
Thymus	3.25	2.63	3.13	2.83	2.94	2.96	0.24
Thyroid	2.52	2.18	2.77	2.29	2.52	2.46	0.23
Urinary Bladder Wall	2.39	2.26	2.86	2.19	2.52	2.44	0.26
Uterus	2.89	2.56	3.30	2.66	3.00	2.88	0.29
Total Body	3.30	3.22	3.39	3.37	3.38	3.33	0.07
Effective Dose (ICRP 103)	4.13	4.32	3.69	4.49	4.28	4.18	0.30

Table 4. Radiation Dosimetry – Male

	Single Participant Individual Organ Dose (μSv/MBq)						
Participant #	**1**	**4**	**5**	**6**	**7**	**Mean**	**St. Dev**
Adrenals	5.71	5.80	5.47	6.28	5.97	5.85	0.30
Brain	1.99	1.80	1.77	1.90	2.09	1.91	0.13
Esophagus	2.69	2.85	2.82	2.90	2.76	2.80	0.08
Eyes	1.62	1.69	1.75	1.62	1.52	1.64	0.09
Gallbladder Wall	6.64	7.21	6.50	7.60	7.89	7.17	0.60
Left colon	2.60	2.73	2.75	2.70	2.54	2.66	0.09
Small Intestine	2.70	2.89	2.89	2.80	2.68	2.79	0.10
Stomach Wall	2.81	2.95	2.94	2.99	2.84	2.91	0.08
Right colon	13.70	17.80	16.00	14.40	17.40	15.86	1.80
Rectum	2.11	2.22	2.30	2.15	1.98	2.15	0.12
Heart Wall	4.07	5.61	5.47	6.14	6.03	5.46	0.83
Kidneys	16.30	14.90	13.10	18.40	16.10	15.76	1.95
Liver	19.90	20.90	19.10	22.80	22.60	21.06	1.63
Lungs	2.55	2.44	2.31	2.78	2.60	2.54	0.18
Pancreas	3.37	3.58	3.52	3.60	3.47	3.51	0.09
Prostate	2.14	2.26	2.33	2.20	2.02	2.19	0.12
Salivary Glands	1.84	1.91	1.98	1.84	1.73	1.86	0.09
Red Marrow	2.00	2.09	2.12	2.08	1.95	2.05	0.07
Osteogenic Cells	1.87	1.95	1.99	1.91	1.79	1.90	0.08
Spleen	4.47	4.17	4.26	4.36	5.00	4.45	0.33
Testes	1.72	1.81	1.89	1.73	1.59	1.75	0.11
Thymus	2.20	2.36	2.39	2.36	2.22	2.31	0.09
Thyroid	1.95	2.03	2.09	1.99	1.84	1.98	0.09
Urinary Bladder Wall	2.02	2.12	2.36	2.59	1.92	2.20	0.27
Total Body	2.39	2.51	2.52	2.50	2.37	2.46	0.07
Effective Dose (ICRP 103)	3.34	3.63	3.44	3.64	3.65	3.54	0.14